



Effects of PCM Mass on Heat Dynamics and Thermal Performance of Solar Air Heaters: A Numerical and Analytical Study

 Ehsan Hasan Zaim^a, Hadi Farzan^{b*}
^a Department of Mechanical Engineering, School of Engineering, Sirjan University of Technology, P. O. Box: 78137-33385, Sirjan, Kerman, Iran.

^b Department of Mechanical Engineering, School of Engineering, Higher Education Complex of Bam, P. O. Box: 76615-314, Bam, Kerman, Iran.

PAPER INFO

Paper history:

Received 04 December 2020

Accepted in revised form 18 May 2021

Keywords:

 Solar Air Heater,
Phase Change Material,
Analytical Study,
Thermal Performance,
Heat Dynamics

ABSTRACT

Utilizing thermal storage units such as Phase Change Materials (PCMs) is a suitable approach to improving Solar Air Heaters (SAHs). The present study tries to assess the effects of PCM mass values on the heat dynamics and thermal performance of SAHs. To this aim, an analytical thermodynamic model was developed and validated by available experimental data. This model provides a robust numerical framework to model the phase change phenomenon and analyze the heat dynamics and thermal performance of SAH using various PCM masses. Four scenarios were considered using the developed analytical model including SAHs using 0, 30, 60, 90 kg PCM. The obtained results illustrated that the maximum outlet temperature was reduced, approximately near 20 %, by increasing the PCM mass between 0 and 90 kg; however, heating time was extended to periods when solar energy availability was inadequate. The thermal performance improved by nearly 14.5 % in the SAH using 90 kg PCM mass compared to the SAH without using PCM. The thermal performance of the SAH with 90 kg PCM was slightly higher than the SAH using 30 kg of PCM; hence, a significant portion of stored thermal energy was lost during nighttime through heat exchange with ambient surroundings. The obtained results also showed that despite available latent thermal energy, the outlet air temperature profiles for the SAHs using different PCM mass were close after sunset due to the low thermal conductivity of paraffin.

<https://doi.org/10.30501/jree.2021.259570.1169>

1. INTRODUCTION

Besides environmental pollution concerns, sustainable growth urges many countries to substitute fossil fuels with renewable and clean energy resources [1]. Solar energy attracts many researchers, engineers, and investors among available renewable energy sources due to its inexhaustibility and pollution-free nature. However, solar energy is not available at night and on cloudy or rainy days. Solar Air Heaters (SAHs) with integrated PCM blocks offer a feasible and inexpensive alternative to collect solar energy, store excess energy, and release it when required. These collectors operate based on extracting thermal energy from hot absorber plates, charging PCM blocks during daytime hours, and delivering stored thermal energy at nighttime hours.

Due to the simplicity and vast applications, numerous studies extensively paid attention to solar heaters and investigated the heat dynamics and thermal performance of these collectors [2-5]. Charvat et al. [6] carried out a numerical and experimental study of PCMs usage as thermal storage units in air-based solar thermal systems to shave peak demand. Shalaby et al. [7] summarized methods used to enhance PCM thermal conductivity, particularly paraffin waxes. Bouadila et al. [8] and Salih et al. [9] experimentally

investigated the effects of mass flow rate on absorbed and recovered heat in a solar air heater with integrated capsulated PCMs. Navarro et al. [10] conducted a research study using latent heat storage to reduce energy consumption for heating purposes in domestic applications. The importance of using PCM on the heat dynamics and thermal performance of SAH was experimentally investigated using two SAHs without and with using thermal storage units [11]. Jain and Tewari [12] investigated the effects of using PCM in a solar crop dryer to keep drying continuity and improve the color and flavor of dried herbs. The energy and exergy efficiency of a single-pass double-glazed solar air heater with packed bed paraffin waxes were investigated at two different mass flow rates [13, 14]. The results illustrated that the daily energy and exergy efficiency varied in ranges from 20.7 % to 26.8 % and from 10.7 % to 19.5 %. In a review study, Khan et al. [15] represented the classification of various PCMs to obtain the long-term durability of latent storage systems. Moradi et al. [16] developed a numerical transient model to investigate the effects of paraffin's thermal conductivity, paraffin's mass, and air mass flow rate on thermal performance. The heat dynamics and performance of a solar air heater using a two-packed bed absorber were investigated by comparing operating time and hot outlet temperature. This study reported that the daily thermal efficiency reached around 47 % [17]. A solar heater using PCMs with honeycomb structure in the PCM panels was

*Corresponding Author's Email: hadi.farzan@bam.ac.ir (H. Farzan)
URL: http://www.jree.ir/article_130708.html



compared with conventional SAHs using PCM to investigate the introduced honeycomb impacts on the thermal performance of SAHs [18, 19]. The acquired experimental results showed that the honeycomb structure reduced charge/discharge time but slightly decreased the average daily performance. Raj et al. [20] investigated a double-pass SAH using encapsulated PCMs and examined the role of geometries of capsules in SAH's heat dynamics of SAH and the charge/discharge process. Jawad et al. [21] suggested adding aluminum chips and tubes with nano-silicon carbide into paraffin wax used in solar heaters to improve their thermophysical properties. Different configurations of absorber plates with embedded capsulated paraffin wax were studied to optimize the thermal performance of SAHs integrated with PCMs [22]. Reddy et al. [23] developed a validated numerical model to study the phase change characteristics and charge/discharge operation in SAHs using PCM blocks.

Phase change modeling in investigating the heat dynamics of SAHs using PCMs is a crucial factor in performing an accurate and precise analysis. Reddy et al. [23] used the enthalpy-porosity technique, while Charvat et al. [24] employed the effective heat capacity method to consider various PCM phases. Summer et al. [25] utilized a lumped parameter model to achieve the temperatures and heat fluxes in a solar collector using PCM. Some studies only used a simple model to obtain the stored thermal energy in PCM [13, 14]. Moradi et al. [16] and Salih et al. [9] used the enthalpy method to model the phase change problem in SAHs with integrated PCMs. All these models are characterized by certain pros and cons and an accurate framework to model the phase change problem with different computational costs. However, these models were tested under extensively different input parameters.

As illustrated in the literature review, early and recent studies have mainly investigated improving SAHs' thermal performance by using phase change materials and compared the heat dynamics of conventional SAHs with SAHs utilizing PCM blocks. These studies assessed the thermal performance of SAHs by concentrating on the technical specifications such

as different absorber configurations, using PCMs' thermal conductivity enhancement, or operational conditions such as charge/discharge durations, air mass flow rate, and inlet air temperature. The current study attempts to assess a crucial technical factor as PCM mass affects SAHs' heat dynamics, such as outlet air temperature, charge/discharge process, and operating duration after sunset. The phase change problem was solved based on a model introduced by Leoni and Amon [26]. This model is an accurate and robust approach to simulating the phase change phenomenon in latent thermal storage units considering the computational cost.

An analytical model was then developed and validated by experimental results, to this aim. The used experimental data were based on an experimental study reported in [11]. Four scenarios were considered using the validated analytical model as a robust framework including SAH without using PCM, SAHs using 30 kg, 60 kg, and 90 kg PCM. The acquired results were analyzed and compared to assess the effects of used PCM mass on the heat dynamics and thermal performance of SAHs.

2. ANALYTICAL MODEL

The experimental approach is an expensive and time-consuming method and, in some cases, needs technical changes in experimental setups. The analytical model provides this opportunity to assess the effects of PCM mass value on the heat dynamics and thermal performance of the collector under study. Experimental data then validated the developed analytical model to examine its accuracy and robustness. The experimental runs were carried out at Tunisia (Longitude $10^{\circ}25'$ E, Latitude $36^{\circ}43'$ N) during August 27th and 28th. The experiments began from 6:00 to 18:00 (local time) and continued throughout the night from 18:00 to 6:00 (next day). The air mass flow rate was 0.018 kg/s, and the calculated Reynolds number implied that the airflow regime was laminar. The SAH studied in [11] used 60 kg paraffin as latent heat storage. Figure 1 shows the schematic of the modeled SAH.

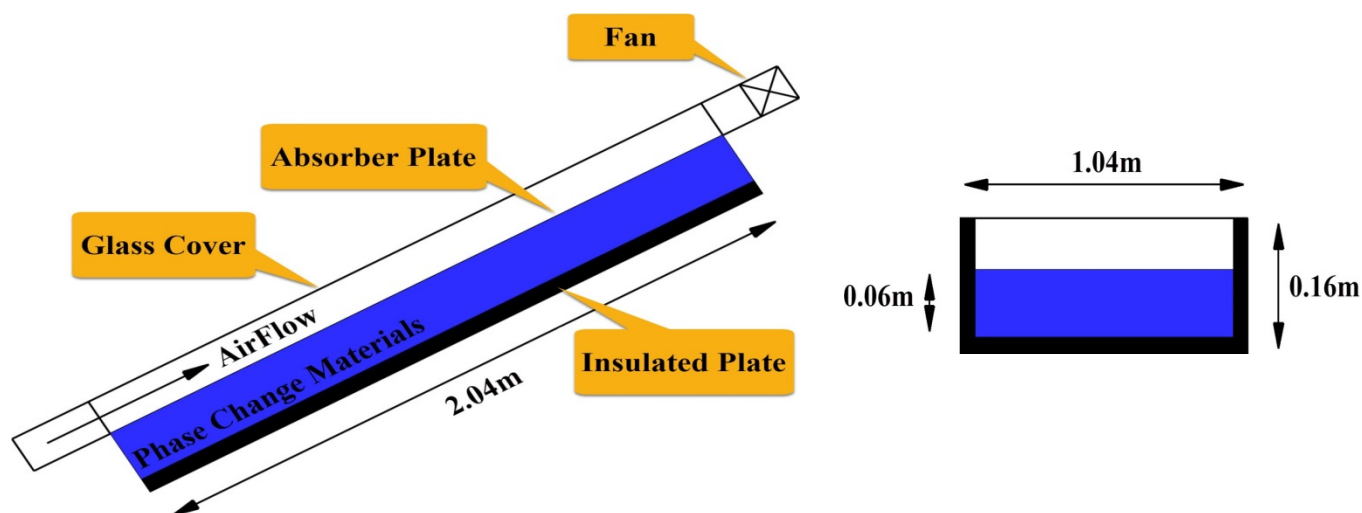


Figure 1. Schematic of solar air heater under study

To simplify the analytical model, the following assumptions were considered:

- The system is operating under quasi-steady-state conditions.
- The airflow regime inside the collector is laminar based on the reported experimental data.
- The inlet air temperature is equal to the ambient air temperature.

- The temperature distribution through the absorber plate and glass cover is considered uniform.
- The collector has heat exchange with its surroundings only through its top surface.
- The phase change problem is one dimensional and occurs in the PCM thickness direction.
- The thermophysical properties of PCMs are constant and do not depend on temperature.

The used thermal network and its associated thermal resistances are shown in Figure 2.

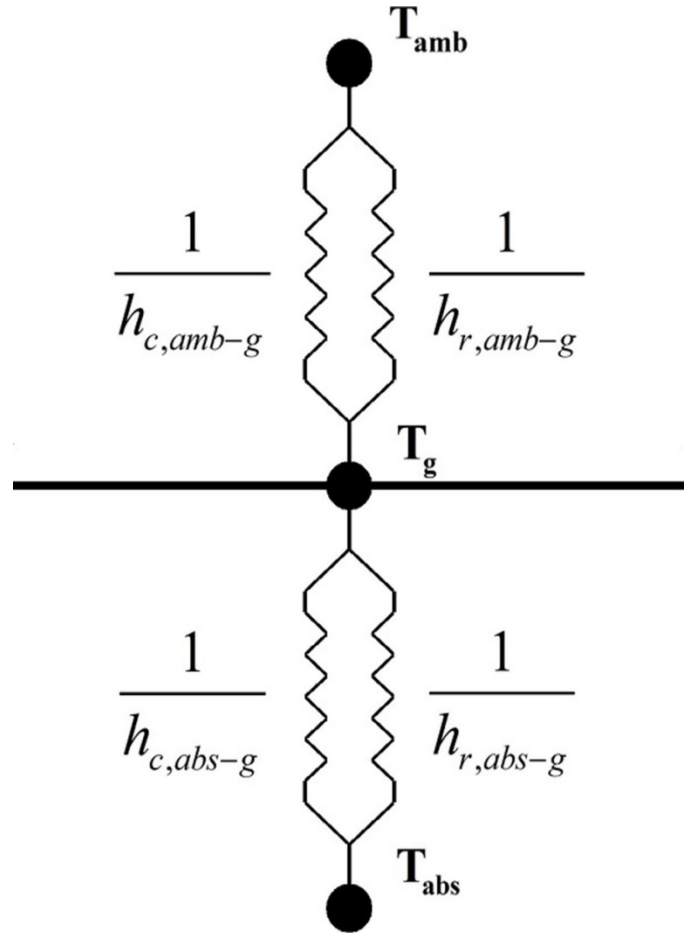


Figure 2. Thermal network of SAH

The reported heat transfer coefficients in Eq. (3) are comprehensively discussed in Table 1.

The total collector heat gain is the amount of heat extracted by the collector exposed to solar irradiation. The energy balance can be utilized to obtain total heat gain and it indicates the distribution of incident solar energy into useful energy gain, thermal energy storage, thermal losses, and optical losses. By using energy balance, total energy gain can be written as follows:

$$Q_{total} = A_c [S - U_L (T_{pm} - T_a)] \quad (1)$$

where Q_{total} and U_L are the total energy gain and heat transfer coefficient, respectively, while A_c is the collector surface area. T_{pm} and T_a represent the mean absorber plate temperature and ambient temperature. S indicates the solar radiation absorbed by a collector per unit area of the absorber and obtains as follow:

$$S = I (\tau\alpha) \quad (2)$$

Here, I is the solar irradiation measured by the installed pyranometer. $\tau\alpha$ is the transmittance-absorptance product and comprehensively discussed in [27]. All collector surfaces were insulated, and only the top one had heat exchange with the surrounding. Hence, U_L can be assumed to equal U_t in which U_t is the top heat loss coefficient. Using thermal network (from ambient air to absorber plate), the top heat loss coefficient, U_t , is obtained as:

$$U_t = \left[\frac{1}{h_{c,abs-g} - h_{r,abs-g}} + \frac{1}{h_w - h_{r,g-a}} \right]^{-1} \quad (3)$$

Table 1. Heat transfer coefficients and calculation formulas

Heat transfer coefficient	Definition	Calculation formula
$h_{c,abs-g}$	Convective heat transfer coefficient between the absorber plate and glass cover	$Nu_{abs-g} \frac{L}{k_a}$
$h_{r,abs-g}$	Radiant heat transfer coefficient between the absorber plate and glass cover	$\frac{\sigma(T_{abs}^2 + T_g^2)(T_{abs} + T_g)}{\frac{1}{\epsilon_{abs}} + \frac{1}{\epsilon_g} - 1}$
$h_{c,g-amb}$	Convective heat transfer coefficient between the glass cover and ambient air [28]	$5.67 + 3.8 v_a$
$h_{r,g-amb}$	Radiant heat transfer coefficient between the glass cover and ambient air	$\epsilon_g \sigma (T_{sky}^2 + T_g^2) (T_{sky} + T_g)$

The sky temperature is given as follows [28]:

$$T_{sky} = 0.0552 T_a^{1.5} \quad (4)$$

Using the energy balance, Eq. (1), the total heat gain was calculated. The total heat gain consists of two main parts given as:

$$Q_{total} = Q_u + Q_{st} \quad (5)$$

where Q_u and Q_{st} denote the useful energy gain and thermal energy stored in PCM blocks. The useful collector heat gain is the amount of heat extracted by the flowing air and given as:

$$Q_u = \dot{m} a c_{p,a} (T_{a,out} - T_{a,in}) \quad (6)$$

Figure 3 represents the energy flow between all elements of the solar heater under study. As shown in Figure 3, the flowing air exchanges heat with the glass cover and absorber plate. By using the energy balance, the useful energy gain by the flowing air can be rewritten as follows:

$$Q_u = h_{c,g-a} A_c (T_g - T_{a,m}) + h_{c,abs-a} A_c (T_{abs} - T_{a,m}) \quad (7)$$

Here, T_g and $T_{a,m}$ are the glass cover temperature and mean flowing air temperature, respectively. The mean flowing air temperature, $T_{a,m}$, inside the collector is obtained as:

$$T_{a,m} = \frac{T_{a,in} - T_{a,out}}{2} \quad (8)$$

where $h_{c,g-a}$ and $h_{c,abs-a}$ are the convective heat transfer coefficients between the flowing air, glass and absorber plate, respectively. To simplify calculations, the heat transfer coefficients between the flowing air, glass cover, and absorber plate are considered equal as given by Eq. (4) in the following:

$$h_c = \frac{Nu \times k_f}{D_k} \quad (9)$$

Here, k_f is the thermal conductivity of flowing air. The Nusselt number for laminar forced convection flow, Nu , can be obtained as [28]:

$$Nu = 4.9 + \frac{0.0606 \left(\frac{RePrD_h}{L} \right)^{1.2}}{1 + 0.0909 \left(\frac{RePrD_h}{L} \right)^{0.7} Pr^{0.17}} \quad (10)$$

$$D_h = \frac{4 (\text{Flow Area})}{\text{Wetted Perimeter}} \quad (11)$$

where Re is the Reynolds number, and Pr denotes the Prandtl number. D_h is the hydraulic diameter. Flow area and wetted perimeter are the area and perimeter of the flowing cross-section, respectively.

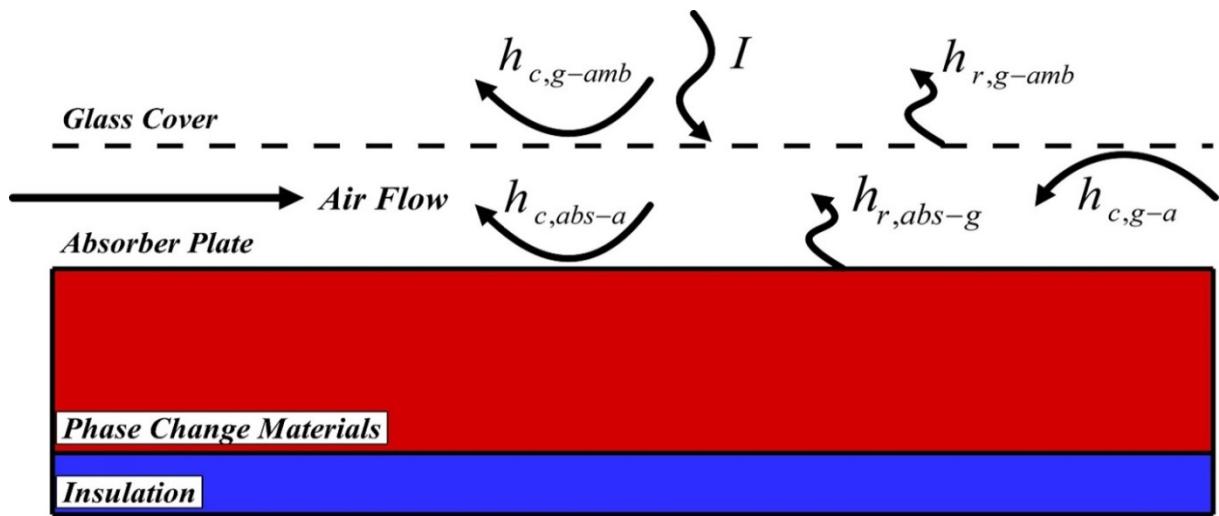


Figure 3. Schematic diagram of energy flow between collector elements

2.1. Phase change modeling

The analytical model used 60 kg paraffin as the latent heat storage unit based on the experimental setup. PCM energy content includes two main parts, including sensible and latent heat contents as follows:

$$E_{PCM} = E_{PCM, \text{Sensible}} + E_{PCM, \text{Latent}} \quad (12)$$

The latent heat content changes to the sensible heat content and vice versa in the charge/discharge process. Phase change modeling in the current study is based on the transient one-dimensional heat transfer equation that includes an internal heat source, given below [24]:

$$\rho_{PCM} c_{p,PCM} \frac{\partial T_{PCM}}{\partial t} = \frac{\partial}{\partial x} \left(k_{PCM} \frac{\partial T_{PCM}}{\partial x} \right) - \dot{Q} \quad (13)$$

Here, ρ_{PCM} , $c_{p,PCM}$ and k_{PCM} denote the density, specific heat capacity, and thermal conductivity of phase change materials, respectively. \dot{Q} is the internal heat source given below [24]:

$$\dot{Q} = \rho_{PCM} L_{f,PCM} \frac{\partial f_{PCM}}{\partial t} \quad (14)$$

where $L_{f,PCM}$ denotes the PCM latent heat and f is the molten mass fraction. By solving the phase change problem, the PCM molten mass fraction and temperature distribution in PCM were calculated at each time interval. The mathematical procedure to solve the phase change problem was comprehensively discussed in [24]. The thermophysical properties of PCM (paraffin wax) are represented in Table 2.

Table 2. Thermophysical properties of PCM [29]

Material	Melting temperature (°C)	Latent heat (J/kg)	Thermal conductivity (W/m K)	Specific heat (J/kg K)		Density (kg/m ³)	
				Liquid	Solid	Liquid	Solid
Paraffin	60	214400	0.21	3890	2940	775	850

The energy balance equations for the solar air heater and flowing air inside the collector in conjunction with the phase change problem were simultaneously solved by EES software in a trial and error procedure. Figure 4 shows the schematic

diagram of the phase change problem and the associated boundary conditions. Using heat balance analysis for each element in the computational domain, we have:

$$q_{PCM,i} - q_{PCM,i+1} = \frac{dU_{PCM,i}}{dt} \quad \text{for } i = 1, 2, \dots, n-1 \quad (15a)$$

$$q_{PCM,i} = k_{PCM} A_{PCM} \frac{(T_{PCM,i} - T_{PCM,i+1})}{l} \quad (15b)$$

$$BC \begin{cases} Q_{st} = k_{PCM} A_{PCM} \frac{(T_{abs} - T_{PCM,1})}{l/2} \\ q_{PCM,n} = 0 \end{cases} \quad (15c)$$

Here, U defines PCM internal energy. k_{PCM} and A_{PCM} are the thermal conductivity and surface area of the integrated PCM. q is the heat exchange rate at two adjacent node interfaces and l denotes the distance between two adjacent nodes. The initial temperature distribution through the PCM was assumed 30 °C. Here, $\frac{dU_{PCM,i}}{dt}$ shows the thermal energy variation and is equal to:

$$\begin{aligned} \frac{dU_{PCM,i}}{dt} &= m_{PCM} c_{p,s} \frac{dT_{PCM}}{dt} & f = 0, \text{ for } T_{PCM,i}^t < T_m \\ &= m_{PCM} c_{p,s} (T_{PCM,i}^{t+1} - T_{PCM,i}^t) \end{aligned} \quad (16a)$$

$$\begin{aligned} \frac{dU_{PCM,i}}{dt} &= m_{PCM} L_{PCM,f} \frac{df}{dt} & 0 < f < 1, \text{ for } T_{PCM,i}^t = T_m \\ &= m_{PCM} L_{PCM,f} (f_i^{t+1} - f_i^t) \end{aligned} \quad (16b)$$

$$\begin{aligned} \frac{dU_{PCM,i}}{dt} &= m_{PCM} c_{p,l} \frac{dT_{PCM}}{dt} & f = 1, \text{ for } T_{PCM,i}^t > T_m \\ &= m_{PCM} c_{p,l} (T_{PCM,i}^{t+1} - T_{PCM,i}^t) \end{aligned} \quad (16c)$$

where $c_{p,s}$ and $c_{p,l}$ are the liquid and solid specific heat capacities of PCM, respectively. The PCM temperature in the i th node, $T_{PCM,i}$, was obtained at each time step based on its calculated heat content. It is worth noting that after and before the melting process, there was a linear relationship between the PCM temperature and its heat content for each node (Eqs. 16a and 16c). However, in the phase change process, the PCM temperature remained constant until the molten mass fraction reached one (16b). Equations (15) to (16) were simultaneously solved to obtain the PCM temperature and molten mass fraction. By solving the governing equations, outlet air and absorber plate temperatures, useful heat gain, and molten mass fraction were obtained.

Since the change in the PCM mass resulted in variations in the storage unit volume, only the PCM thickness would be altered to handle this problem, while the other two dimensions were constant. This issue caused the hydraulic and technical features of the modeled SAH such as absorber surface area and air channel cross-section which did not change in the different considered scenarios.

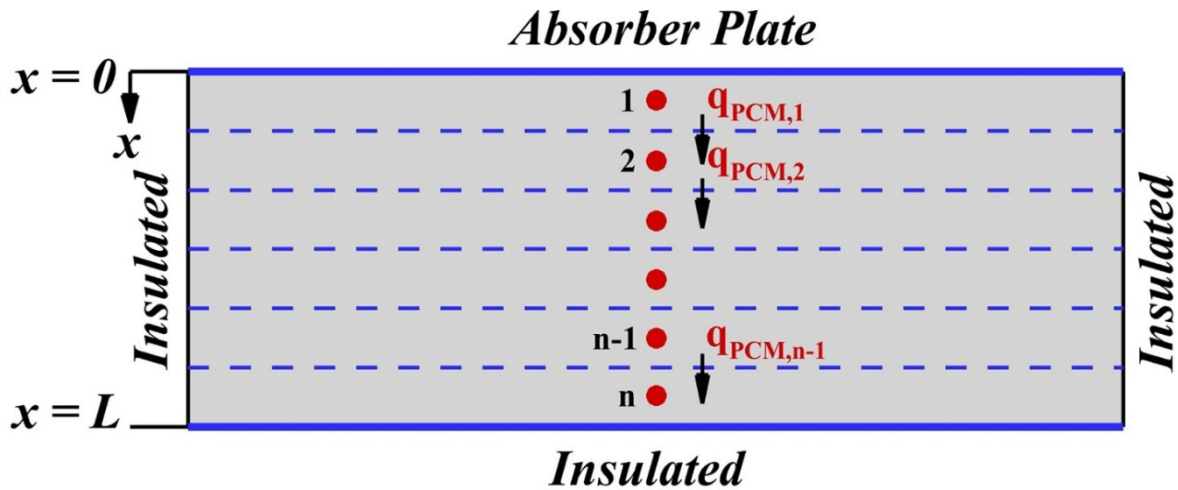


Figure 4. Schematic diagram of the phase change problem and the associated boundary conditions

2.2. Analytical model validation

Figure 5 shows a comparison of the measured and experimental data reported in [11] with the obtained analytical data by the developed model. As seen in Figure 5, there is good agreement between the experimental and analytical data. The percentage mean absolute error (PAME) was used to ensure the accuracy and validity of the analytical method. The PAME is described as follows [30]:

$$PAME = \frac{100}{n} \sum_{i=100}^n \left| \frac{T_{Analyt,i} - T_{Exp,i}}{T_{Exp,i}} \right| \quad (17)$$

where $T_{Analyt,i}$ and $T_{Exp,i}$ are the i th analytical and experimental temperature values, while n denotes temperature values. The PAME is obtained 3.52 % for the set of measured and calculated outlet temperatures that illustrates the accuracy and preciseness of the obtained analytical data.

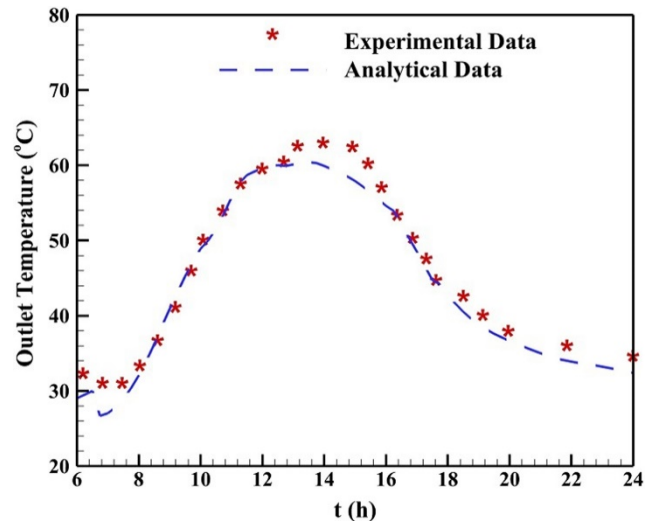


Figure 5. Comparison of available experimental data and obtained analytical data [11]

3. RESULTS AND DISCUSSION

The current study attempts to investigate the effects of PCM mass values on the heat dynamics and thermal performance of SAH using PCM blocks as thermal storage units. To this aim, an analytical model was then developed and validated using available experimental data to assess the effects of PCM mass values on the thermal dynamics of the constructed SAHs. Since the change in the PCM mass resulted in the change in the storage unit volume, only the PCM thickness was altered to handle this problem, while the other two dimensions remained constant. This issue is the reason why the hydraulic and technical features of the modeled SAH, such as absorber surface area and air channel cross-section, did not change in the different considered scenarios.

Environmental conditions such as ambient air temperature and solar intensity can significantly affect the thermal performance of SAHs. Hence, these parameters were monitored and recorded during the experimental runs reported in [11]. Figure 6 represents these measured ambient factors. According to Fig. 6, the ambient air temperature was close to 12 °C at 6:00 and increased to 34 °C until 11:30. The air temperature then began to decrease to approximately 26 °C at 24:00. In the same trend, the solar intensity was zero W/m² at 6:00, increased to near 750 W/m² at 13:00, and then reduced to zero at 19:00.

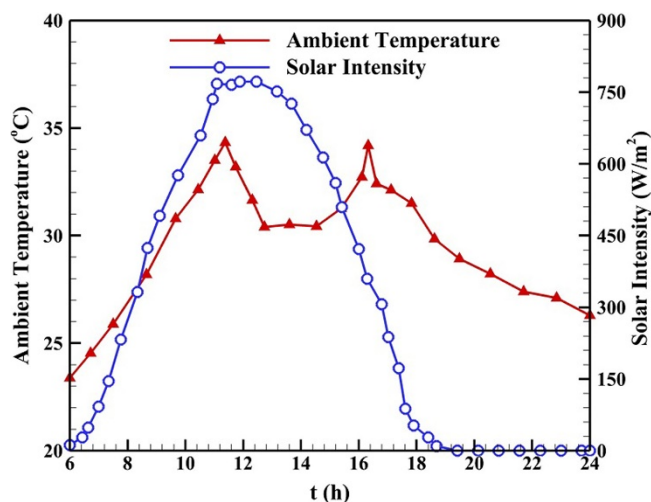


Figure 6. Measured ambient parameters during experimental runs [11]

The outlet temperature is a critical factor that determines the capability of the constructed collector to harvest solar energy. Simply put, the higher the outlet temperature, the higher the SAHs' thermal performance. The developed analytical model was utilized to obtain the heat dynamics and outlet temperature of the constructed SAH using different PCM masses. Figure 7 represents the outlet air temperature using the developed analytical model. As seen in Figure 7, by increasing the PCM mass, the maximum outlet temperature reduced, showing greater thermal energy stored in the PCM blocks instead of heating the flowing air. The maximum reduction in outlet temperature was near 20 °C as the PCM mass varied between 0 kg and 90 kg and occurred in the charging process at around 11:00.

When solar energy availability was not adequate to heat the flowing air, the PCM blocks started to discharge. Figure 7 shows that the SAH containing a higher mass of PCM had higher outlet air temperatures after the sunset. In better words,

due to the higher mass of PCM, more thermal energy was stored and then, released during the periods when solar energy was absent. This issue helps the collector with a higher mass of PCM work for longer periods and extends the heating duration. However, Figure 7 shows that the outlet air temperature profiles for the SAHs using different PCM masses were close at the final hours. It is required to mention that a portion of stored thermal energy heated the flowing air, and the remaining portion was lost to ambient surroundings through convective/radiant heat exchange. The outlet temperature started to reduce in a steeper gradient by discharging the PCM blocks at the late operative time.

Comparison of the outlet air temperature profiles shows that in the SAHs with integrated PCMs, the discharging process began at 16:00 and continued until midnight. The temperature profile for the SAH without the storage unit had a steeper gradient after 16:00 when solar irradiation approached zero; therefore, input thermal energy was inadequate to heating the flowing air. The difference of maximum outlet temperature between the SAH with and without integrated PCMs reached up to near 12 °C. This issue shows the importance of using storage units during the periods when solar irradiation is insufficient.

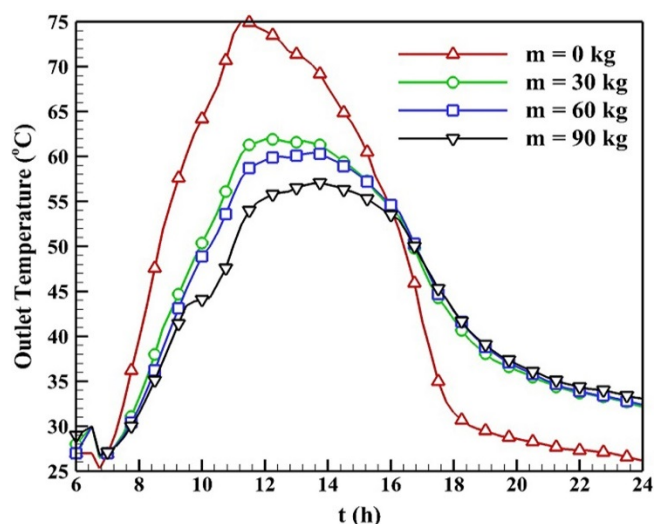


Figure 7. Comparison of outlet air temperature in different considered scenarios

Figure 8 provides an insight into the melting/solidification processes in different considered scenarios using molten mass fraction profiles. As shown in Figure 8, the melting process started at around 9:00 and continued until 18:00; then, the solidification process began. Due to the low thermal diffusivity of paraffin, the heat penetrated slowly into paraffin long after solar intensity peak. Therefore, the melting process continued until 18:00, when solar intensity was negligible. Before 9:00, the input solar energy increased the sensible heat content of the integrated PCM.

Although increasing the PCM mass reduced the mass fraction that melted in the charging process, it improved stored thermal energy. All PCM mass melted in the scenario using 30 kg and this value increased to near 85 kg in the scenario using 90 kg paraffin. In other words, increasing the PCM mass improves the thermal storage capability; this strategy extends the duration that SAHs can perform.

The large amount of PCM was still in the liquid phase at 24:00 according to Figure 8, especially in the SAHs with high PCM amounts, which implied that a large amount of energy

was still stored in PCM. Paraffin's low thermal conductivity resulted in the stored latent energy, which slowly heated the flowing air. This issue is shown in the outlet air temperature profiles. In fact, despite available stored latent energy, the outlet air temperatures in the SAHs using different amounts of PCM masses were so close in the last hours of experimental runs.

This crucial issue is illustrated in Figure 8, representing the melting/solidification process by the molten mass fraction profile.

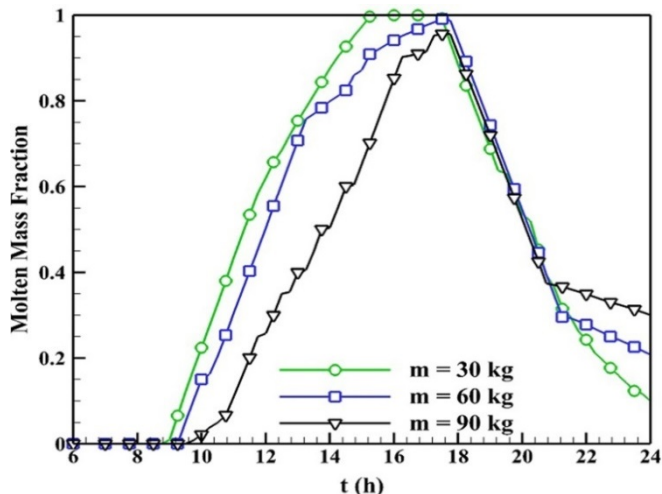


Figure 8. Comparison of charge/discharge process in different considered scenarios

Figure 9 represents the absorber temperature in the different considered scenarios. According to Figure 9, increasing the amount of PCM mass reduced the absorber plate temperature. By increasing the amount of PCM mass, higher absorbed thermal energy was consumed to melt PCM; hence, the absorber plate temperature decreased. This issue had an inherent advantage such as reducing the absorber plate temperature which in turn reduced heat losses in ambient environments.

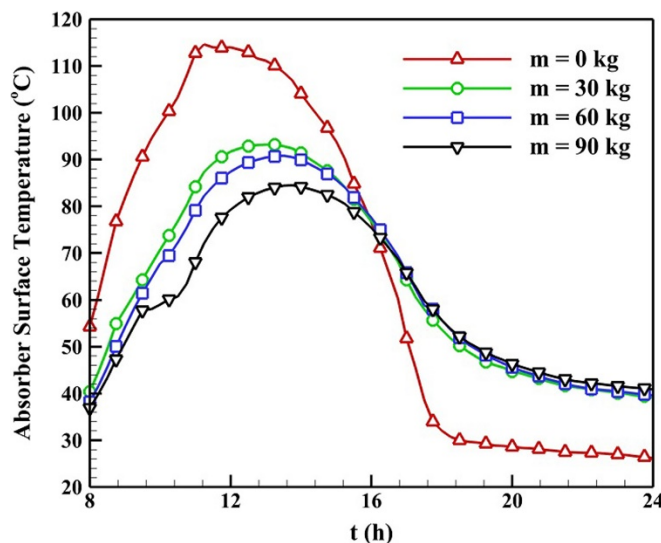


Figure 9. Comparison of absorber temperatures in different considered scenarios

After 18:00, the absorber plate temperature was reduced to 60 °C, the PCM melting temperature. Therefore, the melting process stopped at 18:00, and the solidification process began.

Figure 10 represents the accumulated heat gains in different considered scenarios at each of two hours interval. As represented in Figure 10, heat gains in the SAHs with higher PCM masses are lower than those with lower PCM mass during the daytime. However, during the night, the SAH with the higher mass of PCM represents higher heat gains. This issue proves that the higher amount of PCM mass, the higher the stored energy. The stored energy released during the night and improved the thermal performance of SAHs. It is worth noting that a portion of stored thermal energy was lost due to convective/radiant heat exchange with ambient surroundings. The heat gains data are plotted at every time intervals (two hours).

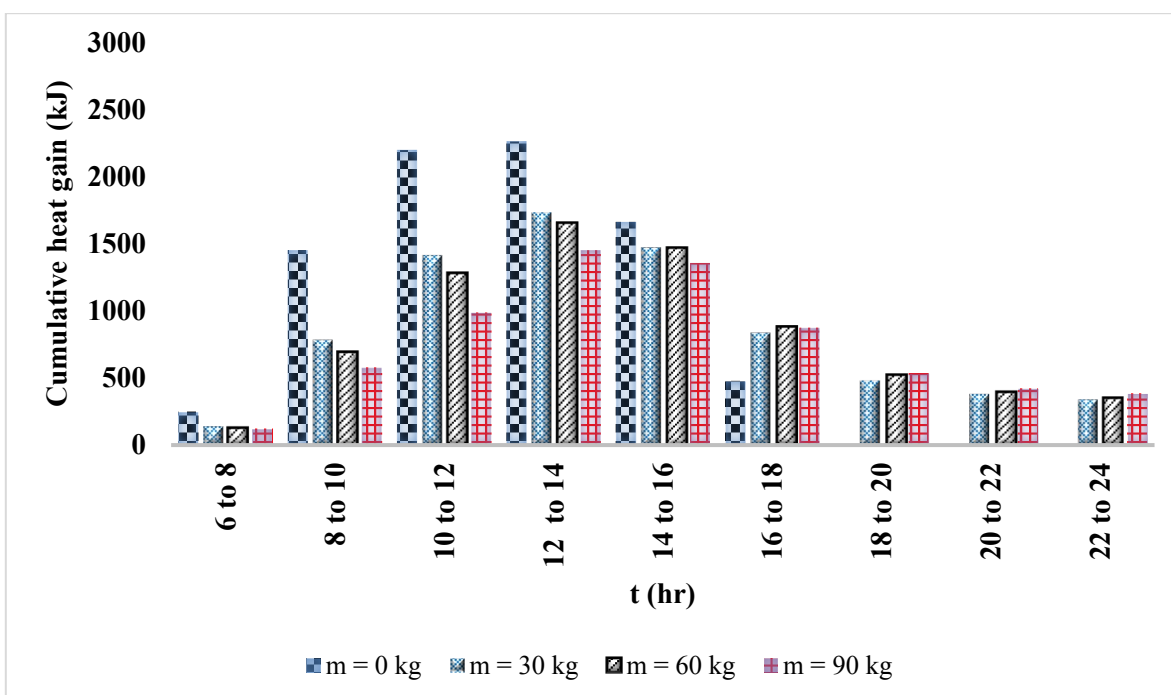


Figure 10. Comparison of accumulated heat gains in different considered scenarios at each of two hours interval

Assessing the daily thermal performance of an energy system is a feasible and useful approach to optimizing the crucial factor affecting the system's performance. In solar thermal systems, the daily thermal performance, η_{Daily} , is defined as the ratio of useful energy gain to received solar energy and given as:

$$\eta_{\text{Daily}} = \frac{\dot{m}c_p \int_{t_1}^{t_2} (T_{a,\text{out}} - T_{a,\text{in}}) dt}{A_t \int_{t_1}^{t_2} I dt} \quad (18)$$

Table 3 shows the daily thermal performance of the SAHs using different PCM masses. As represented in Table 3, the

maximum daily thermal performance belongs to the SAH using 90 kg of PCM and the SAH without using PCM has the lowest thermal performance. By increasing the amount of integrated PCM mass, the SAH's thermal performance slightly improved. Indeed, increasing the PCM increased the stored thermal energy. However, a portion of this stored energy was lost by the absorber plate, SAH framework, and convective/radiant heat exchange with the surroundings. Therefore, the remaining part of the stored energy was consumed to heat the flowing air after the sunset.

Table 3. Daily thermal performance of SAH using different masses of PCM

Scenario	Thermal performance
SAH without using	19.16 %
SAH using 30 kg of PCM	27.01 %
SAH using 60 kg of PCM	28.77 %
SAH using 90 kg of PCM	33.65 %

4. CONCLUSIONS

SAHs with integrated PCMs have been extensively in domestic and industrial applications due to their simple technical structure, low-cost operation and maintenance, and acceptable performance. The current study investigates the effects of PCM mass value on the heat dynamics and thermal performance of SAHs. An analytical model was developed to this aim and validated by available experimental data. The obtained results illustrate that by increasing the PCM mass from zero to 90 kg, the stored thermal energy increased. The stored thermal energy released during nighttime hours and extended the heating process. However, by increasing the PCM mass, the maximum obtained outlet air and absorber plate temperatures were reduced by near 20 °C and 35 °C, respectively. Indeed, the thermal energy that could heat the flowing air was consumed to increase the PCM heat content. Interestingly, the thermal performance improved by increasing the PCM mass from zero to 90 kg by almost 14.5 %. The obtained results showed that despite available latent thermal energy at 24:00, the outlet air temperature profiles for the SAHs using PCM were close due to the low thermal conductivity of paraffin.

5. ACKNOWLEDGEMENT

The authors would like to thank the Sirjan University of Technology and the Higher Education Complex of Bam for their supports.

NOMENCLATURE

A_c	Collector surface area (m ²)
c_p	Specific heat (J/kg.K)
E	Energy (J)
h	Enthalpy (J)
h_w	Wind velocity (m/s)
I	Solar irradiation heat flux (W/m ²)
l	Distance between two adjacent nodes (m)
N_g	Glass number
\dot{m}	Mass flow rate (kg/s)
PAME	Percentage mean absolute errors
q	Heat exchange rate at two adjacent node interfaces (W)
Q_u	Useful energy gain (W)
r	Equivalent thermal energy

S	Absorbed solar intensity (W/m ²)
T	Temperature (°C)
U	Internal energy (J)
U_L	Heat loss coefficient (W/m ² .K)
U_t	Top heat loss coefficient (W/m ²)
V	Wind velocity (m/s)
w	Uncertainty
Greek letters	
β	Tilt angle
ε	Emissivity
η	Efficiency
$\tau\alpha$	Transmittance-absorptance product
Superscripts	
t	Time step
Subscripts	
a	Air
abs	Absorber plate
Analyt	Analytical
cv	Control volume
Exp	Experimental
in	Inlet
out	Outlet

REFERENCES

- Bayati, N., Baghaee, H.R., Hajizadeh, A. and Soltani, M., "Localized protection of radial DC microgrids with high penetration of constant power loads", *IEEE Systems Journal*, (2020), 1-12. (<https://doi.org/10.1109/JSYST.2020.2998059>).
- Daghighi, R. and Shafieian, A., "Thermal performance of a double-pass solar air heater", *Journal of Renewable Energy and Environment (JREE)*, Vol. 3, No. 2, (2016), 35-46. (<https://doi.org/10.30501/jree.2016.70083>).
- Kabeel, A. and Abdelgaied, M., "Solar energy assisted desiccant air conditioning system with PCM as a thermal storage medium", *Renewable Energy*, Vol. 122, (2018), 632-642. (<https://doi.org/10.1016/j.renene.2018.02.020>).
- Patel, J., Shukla, D., Raval, H. and Mudgal, A., "Experimental evaluation of the performance of latent heat storage unit integrated with solar air heater", *International Journal of Ambient Energy*, (2019), 1-9. (<https://doi.org/10.1080/01430750.2019.1636862>).
- SunilRaj, B. and Eswaramoorthy, M., "Experimental study on hybrid natural circulation type solar air heater with paraffin wax based thermal storage", *Materials Today: Proceedings*, Vol. 23, (2020), 49-52. (<https://doi.org/10.1016/j.matpr.2019.06.381>).
- Charvát, P., Klimeš, L. and Ostrý, M., "Numerical and experimental investigation of a PCM-based thermal storage unit for solar air systems", *Energy Buildings*, Vol. 68, (2014), 488-497. (<https://doi.org/10.1016/j.enbuild.2013.10.011>).

7. Shalaby, S., Bek, M. and El-Sebaei, A., "Solar dryers with PCM as energy storage medium: A review", *Renewable Sustainable Energy Reviews*, Vol. 33, (2014), 110-116. (<https://doi.org/10.1016/j.rser.2014.01.073>).
8. Bouadila, S., Lazaar, M., Skouri, S., Kooli, S. and Farhat, A., "Energy and exergy analysis of a new solar air heater with latent storage energy", *International Journal of Hydrogen Energy*, Vol. 39, (2014), 15266-15274. (<https://doi.org/10.1016/j.ijhydene.2014.04.074>).
9. Salih, S.M., Jalil, J.M. and Najim, S.E., "Experimental and numerical analysis of double-pass solar air heater utilizing multiple capsules PCM", *Renewable Energy*, Vol. 143, (2019), 1053-1066. (<https://doi.org/10.1016/j.renene.2019.05.050>).
10. Navarro, L., de Gracia, A., Castell, A. and Cabeza, L.F., "Experimental study of an active slab with PCM coupled to a solar air collector for heating purposes", *Energy Buildings*, Vol. 128, (2016), 12-21. (<https://doi.org/10.1016/j.enbuild.2016.06.069>).
11. El Khadraoui, A., Bouadila, S., Kooli, S., Guizani, A. and Farhat, A., "Solar air heater with phase change material: An energy analysis and a comparative study", *Applied Thermal Engineering*, Vol. 107, (2016), 1057-1064. (<https://doi.org/10.1016/j.applthermaleng.2016.07.004>).
12. Jain, D. and Tewari, P., "Performance of indirect through pass natural convective solar crop dryer with phase change thermal energy storage", *Renewable Energy*, Vol. 80, (2015), 244-250. (<https://doi.org/10.1016/j.renene.2015.02.012>).
13. Ghiami, A., Kianifar, A., Aryana, K. and Edalatpour, M., "Energy and exergy analysis of a single-pass sequenced array baffled solar air heater with packed bed latent storage unit for nocturnal use", *Heat Transfer-Asian Research*, Vol. 46, (2017), 546-568. (<https://doi.org/10.1002/htj.21230>).
14. Ghiami, A. and Ghiami, S., "Comparative study based on energy and exergy analyses of a baffled solar air heater with latent storage collector", *Applied Thermal Engineering*, Vol. 133, (2018), 797-808. (<https://doi.org/10.1016/j.applthermaleng.2017.11.111>).
15. Khan, Z., Khan, Z. and Ghafoor, A., "A review of performance enhancement of PCM based latent heat storage system within the context of materials, thermal stability and compatibility", *Energy Conversion Management*, Vol. 115, (2016), 132-158. (<https://doi.org/10.1016/j.enconman.2016.02.045>).
16. Moradi, R., Kianifar, A. and Wongwises, S., "Optimization of a solar air heater with phase change materials: Experimental and numerical study", *Experimental Thermal Fluid Science*, Vol. 89, (2017), 41-49. (<https://doi.org/10.1016/j.expthermflusci.2017.07.011>).
17. Arfaoui, N., Bouadila, S. and Guizani, A., "A highly efficient solution of off-sunshine solar air heating using two packed beds of latent storage energy", *Solar Energy*, Vol. 155, (2017), 1243-1253. (<https://doi.org/10.1016/j.solener.2017.07.075>).
18. Abuşka, M., Şevik, S. and Kayapınar, A., "Experimental analysis of solar air collector with PCM-honeycomb combination under the natural convection", *Solar Energy Materials Solar Cells*, Vol. 195, (2019), 299-308. (<https://doi.org/10.1016/j.solmat.2019.02.040>).
19. Abuşka, M., Şevik, S. and Kayapınar, A., "A comparative investigation of the effect of honeycomb core on the latent heat storage with PCM in solar air heater", *Applied Thermal Engineering*, Vol. 148, (2019), 684-693. (<https://doi.org/10.1016/j.applthermaleng.2018.11.056>).
20. Raj, A., Srinivas, M. and Jayaraj, S., "A cost-effective method to improve the performance of solar air heaters using discrete macro-encapsulated PCM capsules for drying applications", *Applied Thermal Engineering*, Vol. 146, (2019), 910-920. (<https://doi.org/10.1016/j.applthermaleng.2018.10.055>).
21. Jawad, Q.A., Mahdy, A.M., Khuder, A.H. and Chaichan, M.T., "Improve the performance of a solar air heater by adding aluminum chip, paraffin wax, and nano-SiC", *Case Studies in Thermal Engineering*, (2020), 100622. (<https://doi.org/10.1016/j.csite.2020.100622>).
22. Sudhakar, P. and Cheralathan, M., "Encapsulated PCM based double pass solar air heater: A comparative experimental study", *Chemical Engineering Communications*, (2019), 1-13. (<https://doi.org/10.1080/00986445.2019.1641701>).
23. Reddy, S.S., Soni, V. and Kumar, A., "Diurnal thermal performance characterization of a solar air heater at local and global scales integrated with thermal battery", *Energy*, Vol. 177, (2019), 144-157. (<https://doi.org/10.1016/j.energy.2019.04.017>).
24. Charvát, P., Klimeš, L. and Ostrý, M., "Numerical and experimental investigation of a PCM-based thermal storage unit for solar air systems", *Energy and Buildings*, Vol. 68, (2014), 488-497. (<https://doi.org/10.1016/j.enbuild.2013.10.011>).
25. Summers, E.K. and Antar, M.A., "Design and optimization of an air heating solar collector with integrated phase change material energy storage for use in humidification-dehumidification desalination", *Solar Energy*, Vol. 86, (2012), 3417-3429. (<https://doi.org/10.1016/j.solener.2012.07.017>).
26. Leoni, N. and Amon, C., "Thermal design for transient operation of the TIA wearable computer", *Proceedings of ASME InterPack*, Vol. 2, (1997), 2151-2161.
27. Kalogirou, S.A., *Solar energy engineering: Processes and systems*, Academic Press, (2013). (<https://www.elsevier.com/books/solar-energy-engineering/kalogirou/978-0-12-397270-5>).
28. Duffie, J.A. and Beckman, W.A., *Solar engineering of thermal processes*, fourth edition, John Wiley & Sons, (2013). ([https://www.sku.ac.ir/Datafiles/BookLibrary/45/John%20A.%20Duffie,%20William%20A.%20Beckman\(auth.\)-Solar%20Engineering%20of%20Thermal%20Processes,%20Fourth%20Edition%20\(2013\).pdf](https://www.sku.ac.ir/Datafiles/BookLibrary/45/John%20A.%20Duffie,%20William%20A.%20Beckman(auth.)-Solar%20Engineering%20of%20Thermal%20Processes,%20Fourth%20Edition%20(2013).pdf)).
29. Enibe, S., "Thermal analysis of a natural circulation solar air heater with phase change material energy storage", *Renewable Energy*, Vol. 28, (2003), 2269-2299. ([https://doi.org/10.1016/S0960-1481\(03\)00071-5](https://doi.org/10.1016/S0960-1481(03)00071-5)).
30. O'Hegarty, R., Kinnane, O. and McCormack, S.J., "Concrete solar collectors for façade integration: An experimental and numerical investigation", *Applied Energy*, Vol. 206, (2017), 1040-1061. (<https://doi.org/10.1016/j.apenergy.2017.08.239>).